의학박사 학위논문

Iodine quantification using dual-energy CT: Investigation of the potential sources of measurement variation, calculation of the variability range, and clinical validation of the true enhancement cutoff

이중에너지 전산화단층촬영술을 이용한 요오드 정량화: 측정 변이에 관한 인자 탐색, 측정 변이의 범위 계산 및 임상적 검증

2019 년 2 월

서울대학교 대학원
의학과 영상의학전공
김 형 진

A Thesis of the Degree of Doctor of Philosophy in Medicine

이중에너지 전산화단층촬영술을 이용한 요오드 정량화: 측정 변이에 관한 인자 탐색, 측정 변이의 범위 계산 및 임상적 검증

Iodine quantification using dual-energy CT: Investigation of the potential sources of measurement variation, calculation of the variability range, and clinical validation of the true enhancement cutoff

February 2019

The Department of Radiology,
Seoul National University
College of Medicine

Hyungjin Kim

Abstract

Iodine quantification using dual-energy CT: Investigation of the potential sources of measurement variation, calculation of the variability range, and clinical validation of the true enhancement cutoff

Hyungjin Kim

Department of Radiology, College of Medicine

The Graduate School

Seoul National University

Purpose: To analyze the effect of dual-energy computed tomography (DECT) scanners, acquisition parameters, and fluid characteristics on iodine quantification and to calculate and validate the measurement variability range induced by those variables.

Methods: In Part I and II, experimental studies were performed using four mediastinal iodine phantoms. Phantoms were scanned with three different DECT scanners from major vendors using various acquisition

parameters and their effects on the measurement of iodine density (IoD) were investigated using linear mixed-effect models. Measurement variability range of IoD was also calculated. In Part III, diagnostic usefulness of the true enhancement cutoff was retrospectively validated in patients who underwent surgical resections for thymic cysts and thymic epithelial tumors.

Results: In Part I, absolute error of IoD was not significantly affected by the DECT systems and kind of solvents ($P>0.05$). Measurement variability range was from -0.6 to 0.4 mg/ml for the true iodine concentration 0 mg/ml. In Part II, tube voltage ($P<0.001$) and tube current-time product ($P<0.05$, depending on the interaction terms) had statistically significant effects on IoD. However, the magnitude of their effects was minimal in the range of diagnostic CT scans. Solvents also had significant effects on IoD ($P=0.007$). Specifically, the difference of least squares means between water and amino acid solution ranged from 0.1 to 0.3 for tubes with iodine concentrations ≥5 mg/ml and from -0.4 to -0.1 mg/ml for tubes with iodine concentrations ≤1 mg/ml. Spectral level was not an affecting factor ($P=0.647$). In Part III, the true enhancement cutoff for IoD, which was 0.4 mg/ml, exhibited diagnostic sensitivity, specificity, accuracy, positive predictive value, and negative predictive value of 100%, 85.7%, 90.9%, 80.0%, and 100%, respectively,

for the differentiation of thymic epithelial tumors from thymic cysts.

Conclusions: IoD measurement is robust to the DECT scanners from different vendors. IoD is significantly affected by the acquisition parameters, but the magnitude of effects are minimal in the range of diagnostic CT scans. The true enhancement cutoff of 0.4 mg/ml is an accurate parameter for the differentiation of thymic epithelial tumors from thymic cysts.

Key Words: Iodine quantification; Iodine density; Dual-energy computed tomography; Dual-layer CT; Measurement variability; CT acquisition parameter; Thymic cyst

Student Number: 2017-35354

CONTENTS

LIST OF TABLES AND FIGURES

LIST OF ABBREVIATION

DECT: dual-energy computed tomography
DLCT: dual-layer IQon spectral CT
DSCT: dual-source dual-energy CT
EMR: electronic medical record
HU: Hounsfield units
IoD: iodine density
IRA: iodine-related attenuation
LSM: least squares means
NPV: negative predictive value
PPV: positive predictive value
RME: relative measurement error
ROI: region-of-interest
SSCT: single source dual-energy CT with rapid kilovoltage switching
VME: virtual monoenergetic
VNE: virtual non-enhanced

INTRODUCTION

The development of dual-energy computed tomography (DECT) enabled material-specific imaging, which is also known as material decomposition. Material-specific imaging can be applied to the separation of a number of substances including water, iodine, calcium, uric acid and fat (1). With the use of this technique, users can obtain mass density, effective atomic number, or other material-information (2, 3).

Iodine density (IoD) mapping is a powerful application based on DECT material decomposition as injection of contrast media is routinely performed for the patients with various vascular or oncologic diseases. Distribution of iodinated contrast material can be evaluated qualitatively or quantitatively on images. Pulmonary embolism would be one of the most widely studied disease entities with respect to this imaging technique (4-7). For thoracic applications, iodine quantification has also been investigated for thymic epithelial tumor (8), ischemic heart disease (9, 10), and lung cancer (11-16). Importantly, iodine quantification had significant diagnostic (histology, differentiation, and gene expression) (11, 14-16) as well as prognostic correlation (17, 18) for lung cancer.

Iodine quantification may have benefits over conventional CT attenuation measurement with Hounsfield units (HU). In recent days, CT scanning protocols including contrast media dosage and tube voltage

setting vary substantially depending on the clinical situations and institutional standards. Therefore, it is not easy to determine the enhancement status of lesions based solely on attenuation thresholds. In this context, IoD can be utilized as a surrogate. IoD can facilitate differentiating high attenuation lesions due to past hemorrhage, calcification or pseudoenhancement from true iodine uptake (19-22). In addition, acquisition of non-enhanced CT is not necessary for the comparisons between enhanced and non-enhanced images as IoD reflects iodine content in a given area. However, the robustness of this parameter has not been assessed thoroughly.

For the generalized application of the DECT-based iodine quantification, a prerequisite would be the evaluation of measurement accuracy and reproducibility. Past publications reported that the IoD measurement on DECT was accurate (23-25) and that the inter-reader agreement was excellent among observers (23, 26). Nevertheless, the effect of various DECT scanners, acquisition parameters, or the proteinaceous body fluid, on which the region-of-interest (ROI) is placed, has not yet been reported to date. As the material decomposition algorithms are specific to each vendor, there can be potential variability among multiple CT manufacturers for iodine quantification. The acquisition parameters including tube voltage, tube current-time product, and iterative

reconstruction may also have effects on the measurement.

Therefore, this study aimed to analyze the effect of DECT scanners, acquisition parameters, and fluid characteristics on iodine quantification and to calculate and validate the measurement variability range induced by those variables. This study consisted of the three parts: Part I. Analysis of the effect of DECT scanners and fluid characteristics on iodine quantification; Part II. Analysis of the effect of various acquisition parameters on iodine quantification using a single DECT scanner; and Part III. Clinical validation of the iodine density measurement in patients who underwent surgical resection for thymic cysts or thymic epithelial tumors.

PART I. ANALYSIS OF THE EFFECT OF DECT SCANNERS AND FLUID CHARACTERISTICS ON IODINE QUANTIFICATION

MATERIALS AND METHODS

This study was exempt from Institutional Review Board approval of the Seoul National University Hospital as no animal or human data were acquired or used.

Phantom study

An experimental study was performed with an anthropomorphic chest phantom (multipurpose chest phantom N1 Lungman, Kyoto Kagaku, Japan) containing custom-made mediastinal iodine phantoms. Iodine phantoms were produced with 500 ml cylindrical plastic beakers (diameter and height, 94 and 118 mm; polymethylpentene; Brand, Wertheim, Germany), which had six tubes of different iodine concentrations (0, 1.0, 2.5, 5.0, 10.0, and 20.0 mg/ml). Six tubes were placed upright and circumferentially in the cylindrical beakers and were surrounded by 3% agar gel solution (Figure 1). Four iodine phantoms were prepared and the tubes in each phantom had contrast media (Iopamidol; Pamiray 370, Dongkook Pharmaceutical Co., Seoul, Korea) diluted in four different solvents (water, 10% amino acid solution, 20%

lipid emulsion, and 18% calcium solution; fluid other than water was extracted from Combiflex lipid 1000 inj., JW Pharmaceutical, Seoul, Korea) (Table 1). These solutions were chosen as alternatives for body fluid to simulate in vivo iodine quantification. The iodine phantoms were placed in the mediastinal compartment of the anthropomorphic chest phantom.

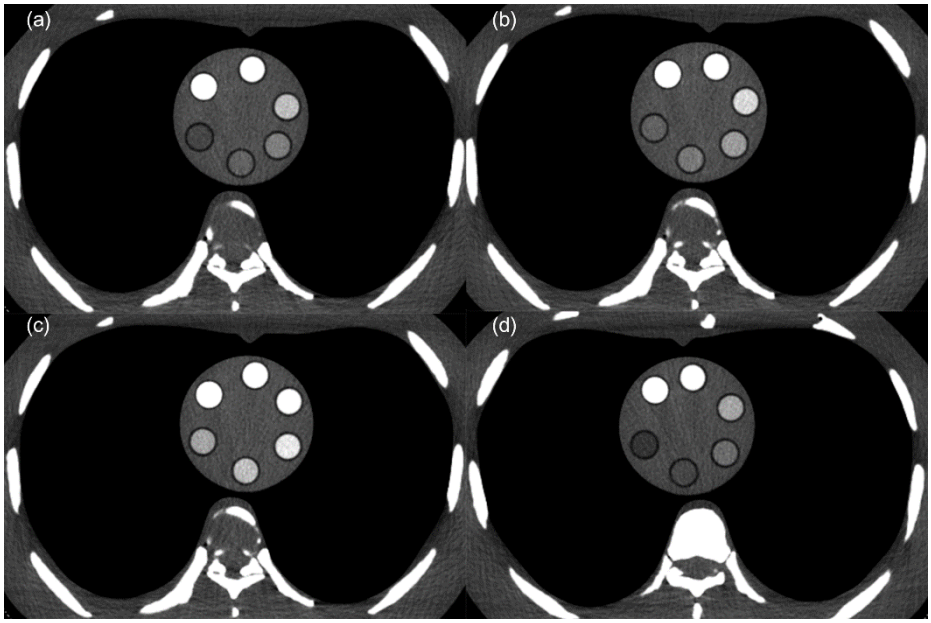

Figure 1. Iodine phantoms which contained six different iodine concentrations (0, 1.0, 2.5, 5.0, 10.0, and 20.0 mg/ml) diluted in (a) water, (b) 10% amino acid solution, (c) 18% calcium solution, and (d) 20% lipid emulsion. Images shown here were obtained with DSCT at volume CT dose index of 7 mGy and at blending ratio of 0.6. Blended images of low- and high-kVp scans were not used in the analysis.

DSCT, dual source dual-energy computed tomography scanner

Table 1. Mediastinal Iodine Phantoms

Mediastinal phantom	**Solvent**	**True iodine concentration (mg/ml)**
1	Water	0, 1.0, 2.5, 5.0, 10.0, 20.0
2	10% amino acid solution	0, 1.0, 2.5, 5.0, 10.0, 20.0
3	20% lipid emulsion	0, 1.0, 2.5, 5.0, 10.0, 20.0
4	18% calcium solution	0, 1.0, 2.5, 5.0, 10.0, 20.0

CT scanning protocols

CT scans were performed with three DECT scanners [dual-layer IQon spectral CT (DLCT), Philips Healthcare, Best, the Netherlands; dual-source DECT (DSCT), SOMATOM Force, Siemens Healthcare, Forchheim, Germany; single source DECT with rapid kilovoltage switching (SSCT), Discovery CT 750 HD, GE Healthcare, Milwaukee, WI, USA]. Scanning protocols were set with near-equivalent acquisition parameters among the three scanners except for the tube voltage. Tube voltages were 140 kVp for DLCT, 80/Sn150 kVp for DSCT, and 80/140 kVp for SSCT. The photon spectra of these three x-ray sources were substantially different (27). For DSCT, 150 kVp with a tin filter was chosen, allowing for slight inequality among protocols. Nonetheless, the availability of higher tube voltage with filtration of lower energy photons through a tin filter was considered as an imperative strength of DSCT scanner and thus it was used for comparisons. The standard DECT protocols for DSCT in Seoul National University Hospital also comprised of the same tube voltage setting. In this study, the only variable among the acquisition parameters was the radiation dosage in terms of volume CT dose index. CT scans were performed at both 3 and 7 mGy (low-dose and regular dose) for the comparison of IoD measurements between radiation dosage settings (28). However, CT

scanning at 3 mGy was not available with SSCT and images were obtained at only 7 mGy for this scanner. Other detailed acquisition parameters are described in Table 2. CT scans were repeated five times with a slight change in position for each iodine phantom. Therefore, a total of 100 CT scans [3 CT scanners x iodine phantoms with 4 different solvents x (2 radiation dose settings for DLCT and DSCT and a single dose setting for SSCT) x 5 repeats] were obtained.

Table 2. CT Acquisition Protocol of each DECT Scanner

DECT scanner	**DLCT**		**DSCT**		**SSCT**
CTDIvol (mGy)	3	7	3	7	7
Scan mode	N/A		Dual energy		GSI 49
Tube voltage (kVp)	140		80/Sn150		80/140
Tube current-time product (mAs)	24	57	80/44	186/103	182
Rotation time (sec)	0.4	0.4	0.5	0.5	0.7
Pitch	1.171	1.171	1.2	1.2	1.375
Detector collimation (mm)	64x0.625	64x0.625	128x0.6	128x0.6	64x0.625
Reconstruction algorithm	Spectral 0[a]		FBP	FBP	FBP
Reconstruction kernel	B (standard)		Qr40		Standard
Slice thickness (mm)	1		1		1.25
Slice increment (mm)	1		1		1.25

[a]Spectral 0 is equivalent to FBP.

CTDIvol, volume CT dose index; DECT, dual-energy CT; DLCT, dual-layer spectral CT; DSCT, dual-source dual-energy CT; FBP, filtered back projection; GSI, Gemstone spectral imaging; SSCT, single-source dual-energy CT with rapid kilovoltage switching

Imaging analysis

IoD (mg/ml), CT attenuation number (HU) at virtual monoenergetic (VME) 70 keV, and CT attenuation number (HU) at virtual non-enhanced images (VNE) were obtained by placing round ROIs of about 100 mm^2 on axial images. VME 70 keV images were regarded as near-equivalent to the conventional polychromatic 120 kVp images (29, 30). Mean values of each parameter were recorded. Measurements were conducted using dedicated software programs of each vendor [Spectral CT viewer of Spectral Diagnostic Suite, Philips Healthcare; Virtual Unenhanced application and Monoenergetic Plus application of Syngo.via software VB10, Siemens Healthcare; Material suppressed iodine application of Gemstone Spectral Imaging viewer, GE Healthcare]. A total of 600 measurements (100 CT scans x 6 tubes per scan) were performed.

Statistical analysis

The measurement accuracy of IoD was analyzed by using a linear mixed-effect model. Fixed effect terms of interest were DECT scanners, kind of solvents, and radiation dosage settings, which were categorical variables. True iodine concentration was also included as a fixed effect term in the model and was regarded as a continuous variable. Repeated CT scans were considered as a random effect, a categorical variable. The dependent variable in the model was the absolute IoD measurement error

and was calculated as follows: |Measured IoD – True iodine concentration|.

To determine the effects of the same fixed effect terms on the CT attenuation numbers, linear mixed-effect models were run again with the following dependent variables: 1) CT attenuation at 70 keV and 2) iodine-related attenuation (IRA; HU at 70 keV minus HU at VNE). The initial models were created with main effect terms with the entry of pairwise interaction terms between fixed effect terms iteratively. Thereafter, the final model was created using main effect terms and statistically significant interaction terms.

Then, the measurement variability range of IoD was investigated. As absolute differences between the measured IoD and true iodine concentration [i.e., (Measured IoD – True iodine concentration)] did not have normal distributions, a non-parametric form of 95% limits of agreement method was used (31). The 95% limits of agreement were defined as 2.5 and 97.5 percentiles of absolute differences (31) and 95% confidence intervals for each percentile were also calculated by bootstrap resampling (1000 samples).

Statistical analyses were performed using SAS version 9.2 (SAS Institute Inc., Cary, NC, USA) and SPSS 19.0 (IBM SPSS Statistics, Armonk, NY, USA). A P-value <0.05 was considered to indicate

statistical significance.

RESULTS

IoD was generally underestimated when measured at DLCT and SSCT (Table 3). However, the under- or overestimation was dependent on the true iodine concentration for DSCT. In other words, for the true iodine concentration ≤1.0 mg/ml, IoD was underestimated for DSCT. However, for the true concentration ≥2.5 mg/ml, DSCT overestimated IoD, unlike the other CT scanners. Relative measurement error was highest at the true concentration of 1.0 mg/ml for all scanners and showed decreasing tendency as the true iodine concentration increased.

Table 3. Absolute Differences of the Iodine Density Measurements according to DECT Scanners

True iodine concentration	DECT scanner	Median of absolute differences	IQR of absolute differences	Median of relative differences[a]	IQR of relative differences[a]
0	DLCT	0	0, 0.1	N/A	N/A
	DSCT	-0.2	-0.3, 0.1	N/A	N/A
	SSCT	-0.1	-0.5, 0.3	N/A	N/A
1.0	DLCT	-0.3	-0.5, 0.1	-30.0	-50.0, 5.0
	DSCT	-0.2	-0.4, -0.1	-20.0	-37.5, 10.0
	SSCT	-0.3	-0.5, -0.1	-29.0	-52.8, 10.5
2.5	DLCT	-0.2	-0.3, 0	-6.0	-12.0, 0
	DSCT	0.2	-0.1, 0.3	6.0	-3.0, 12.0
	SSCT	-0.3	-0.5, -0.1	-10.8	-19.0, -3.1
5.0	DLCT	-0.4	-0.5, 0	-7.0	-10.0, -0.5
	DSCT	0.4	0.1, 0.6	8.0	2.0, 12.0
	SSCT	-0.4	-0.7, -0.2	-8.3	-13.1, -3.8
10.0	DLCT	-0.6	-0.9, -0.2	-6.0	-9.0, -2.0
	DSCT	0.5	0.3, 0.9	5.0	3.0, 9.0
	SSCT	-0.5	-1.0, -0.2	-5.2	-9.8, -1.9
20.0	DLCT	-0.9	-1.0, -0.7	-4.5	-5.0, -3.5
	DSCT	1.0	0.9, 1.2	5.0	4.5, 5.9
	SSCT	-0.7	-1.2, -0.5	-3.4	-6.2, -2.7

Iodine density was measured in mg/ml, unless otherwise specified.

[a]Data are in percentages.

DECT, dual-energy CT; DLCT, dual-layer spectral CT; DSCT, dual-source dual-energy CT; IQR, interquartile range; SSCT, single-source dual-energy CT with rapid kilovoltage switching

Absolute measurement error of IoD according to the DECT scanners and other variables

Absolute measurement error of IoD was not significantly affected by the analyzed fixed effect terms including the CT scanners (P=0.742), kind of solvents (P=0.438), and radiation dosage (P=0.776) (Figure 2). It was only influenced by the true iodine concentration (P<0.001). The estimated regression coefficient of true iodine concentration was 0.037 (standard error, 0.001), which implied that the absolute measurement error increased by 0.037 mg/ml as the true iodine concentration increased by 1.0 mg/ml.

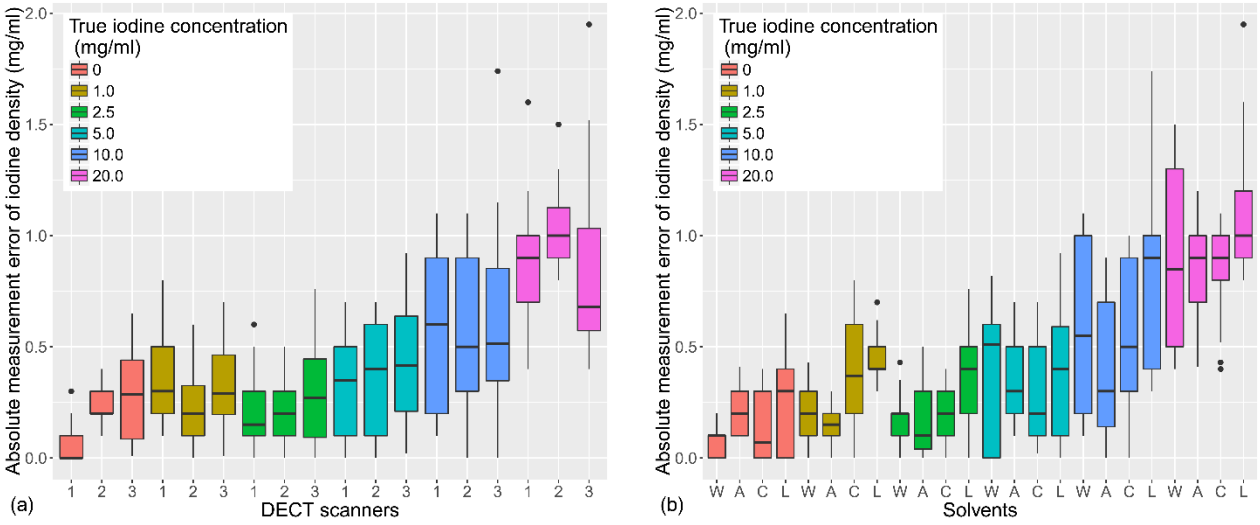

Figure 2: Box plots of absolute measurement error of iodine density according to (a) dual-energy CT scanners and (b) kind of solvents. Both factors were not significantly associated with iodine density measurement accuracy.

Scanner 1, dual-layer IQon spectral CT; scanner 2, SOMATOM Force; scanner 3, Discovery CT 750 HD; solvent W, water; solvent A, 10% amino acid solution; solvent C, 18% calcium solution; solvent L, 20% lipid emulsion.

Although the effect of CT scanners on the measurement accuracy was not significant, SSCT showed a slightly higher absolute measurement error (0.5 mg/ml) than other CT systems (0.4 mg/ml) (Table 4). The measurement error was also higher for the IoD in lipid solution (0.6 mg/ml) than that in other solvents of water, amino acid, and calcium solution (0.4 mg/ml).

Table 4. Estimated Least-squares Means (LSMs) of the Absolute Differences for Iodine Density Measurements

		LSM	**95% CI**	**Difference of LSM**	**95% CI for the difference of LSM**
DECT scanner	DLCT	0.4	0.3, 0.5		
	DSCT	0.4	0.3, 0.6	-0.1[a]	-0.2, 0.1
	SSCT	0.5	0.2, 0.7	-0.1	-0.3, 0.2
Solvent	Water	0.4	0.2, 0.6		
	Amino acid solution	0.4	0.2, 0.6	0	-0.2, 0.3
	Calcium solution	0.4	0.2, 0.6	0	-0.3, 0.2
	Lipid solution	0.6	0.4, 0.7	-0.2	-0.4, 0.1
Radiation dosage (mGy)	3	0.4	0.3, 0.6		
	7	0.4	0.3, 0.5	0	-0.2, 0.2

Iodine density was measured in mg/ml.

[a]This value was 0.050 and was rounded to one decimal place.

CI, confidence interval; DECT, dual-energy CT; DLCT, dual-layer spectral CT; DSCT, dual-source dual-energy CT; SSCT, single-source dual-energy CT with rapid kilovoltage switching

Effect of the DECT scanners and other variables on CT attenuation numbers

CT attenuation number at 70 keV was significantly affected by the CT scanners ($P<0.001$), kind of solvents ($P<0.001$), and true iodine concentration ($P<0.001$). The interaction terms among them were also statistically significant (true iodine concentration*CT scanner, $P<0.001$; true iodine concentration*solvent, $P<0.001$; CT scanner*solvent, $P=0.014$), which implied that the impact of CT scanners on HU was different according to the various true iodine concentrations and kind of solvents. In other words, the effect of CT scanners on HU was not limited to each scanner, but was also dependent on the true iodine concentrations and kind of solvents. Thus, CT attenuation number was affected by the complex, inter-dependent relationship between the three variables. CT attenuation at 70 keV was not significantly associated with the radiation dosage ($P=0.700$). Detailed data are displayed in Table 5.

Table 5. CT Attenuation at VME 70 keV and IRA according to the True Iodine Concentrations and DECT Scanners

		CT attenuation (HU) at VME 70 keV		**IRA (HU)**	
True iodine concentration (mg/ml)	**DECT scanner**	**Median**	**IQR**	**Median**	**IQR**
0	DLCT	19.8	-12.3, 107.0	-0.3	-1.0, 2.2
	DSCT	17.8	-14.7, 99.3	-4.9	-8.3, 2.1
	SSCT	15.1	-21.5, 92.6	0.3	-0.5, 1.9
1.0	DLCT	43.3	11.7, 125.3	18.2	14.1, 28.2
	DSCT	39.6	12.6, 123.2	21.7	18.2, 24.5
	SSCT	32.8	6.1, 111.1	10.4	4.6, 16.4
2.5	DLCT	81.2	50.0, 167.7	63.8	56.6, 67.6
	DSCT	87.3	55.8, 170.6	68.9	63.9, 72.0
	SSCT	65.3	38.5, 145.9	47.9	40.8, 51.8
5.0	DLCT	141.3	111.1, 224.0	121.6	118.8, 130.3
	DSCT	157.4	123.7, 236.5	140.1	132.9, 145.6
	SSCT	121.7	94.2, 208.2	102.8	98.3, 115.9
10.0	DLCT	264.2	228.3, 337.3	248.1	236.8, 257.2
	DSCT	294.0	260.8, 366.4	273.5	267.5, 283.6
	SSCT	242.6	206.6, 317.8	230.5	215.6, 235.6
20.0	DLCT	506.4	479.6, 582.3	502.8	499.8, 507.7
	DSCT	565.8	528.9, 633.6	545.5	542.6, 550.1

	SSCT	473.4	439.3, 550.8	469.8	458.1, 477.3

DECT, dual-energy CT; DLCT, dual-layer spectral CT; DSCT, dual-source dual-energy CT; HU, Hounsfield Unit; IQR, interquartile range; IRA, iodine-related attenuation; SSCT, single-source dual-energy CT with rapid kilovoltage switching; VME, virtual monoenergetic image

IRA was also significantly affected by the CT scanners ($P<0.001$), kind of solvents ($P<0.001$), and true iodine concentration ($P<0.001$) (Figure 3). The interaction terms among them were also statistically significant (true iodine concentration*CT scanner, $P<0.001$; true iodine concentration*solvent, $P<0.001$; CT scanner*solvent, $P<0.001$), which implied that IRA was associated with the inter-dependent relationship between the three variables. IRA was not significantly associated with the radiation dosage ($P=0.577$). Detailed data are described in the Table 6.

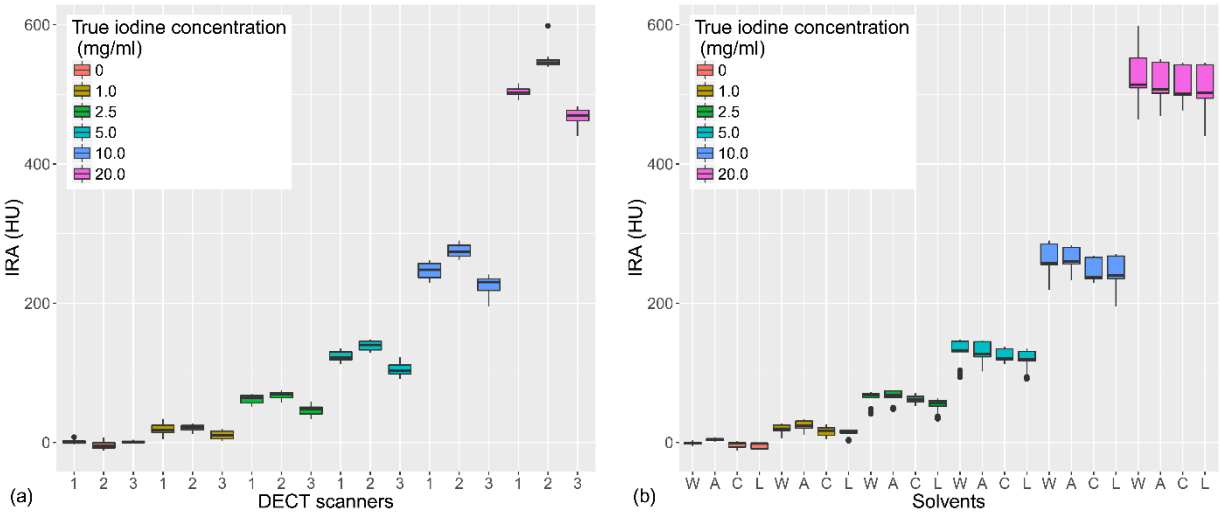

Figure 3: Box plots of iodine-related attenuation (IRA; HU at 70 keV minus HU at VNE) according to (a) dual-energy CT scanners and (b) kind of solvents. IRA was significantly affected by the CT scanners and solvents.

HU, Hounsfield units; scanner 1, dual-layer IQon spectral CT; scanner 2, SOMATOM Force; scanner 3, Discovery CT 750 HD; solvent W, water; solvent A, 10% amino acid solution; solvent C, 18% calcium solution; solvent L, 20% lipid emulsion; VNE, virtual non-enhanced image.

Table 6. CT Attenuation at VME 70 keV and IRA according to the True Iodine Concentrations and Solvents

		CT attenuation (HU) at VME 70 keV		**IRA (HU)**	
True iodine concentration (mg/ml)	**Solvent**	**Median**	**IQR**	**Median**	**IQR**
0	Water	-2.0	-4.0, -0.3	-0.7	-2.4, 0.3
	10% amino acid solution	38.6	37.3, 39.7	4.1	2.9, 5.7
	18% calcium solution	123.5	119.8, 130.8	-1.1	-6.7, 0.1
	20% lipid emulsion	-18.9	-20.6, -18.0	-1.5	-9.0, -1.0
1.0	Water	21.7	20.4, 24.3	19.7	16.5, 25.1
	10% amino acid solution	57.2	54.5, 64.7	24.0	20.1, 30.9
	18% calcium solution	146.7	144.9, 148.7	17.1	10.4, 21.3
	20% lipid emulsion	6.2	3.5, 7.5	15.5	13.0, 17.5
2.5	Water	64.9	61.3, 68.0	68.0	64.3, 69.9
	10% amino acid solution	102.3	98.6, 105.3	68.3	64.3, 74.3
	18% calcium solution	192.1	189.2, 194.3	61.4	57.7, 66.5
	20% lipid emulsion	45.5	42.9, 48.2	56.3	51.5, 60.2
5.0	Water	128.3	124.8, 139.7	132.1	130.3, 145.5
	10% amino acid	156.9	154.2, 172.9	127.4	122.8, 144.9

	solution				
	18% calcium solution	249.5	246.0, 258.8	120.7	118.1, 134.6
	20% lipid emulsion	106.2	101.2, 116.3	119.3	116.3, 131.2
10.0	Water	250.3	245.6, 279.2	257.9	255.2, 286.2
	10% amino acid solution	281.9	278.0, 307.4	259.9	256.0, 280.1
	18% calcium solution	361.1	356.6, 386.4	237.0	234.4, 266.1
	20% lipid emulsion	221.3	217.6, 251.9	240.0	235.1, 268.0
20.0	Water	494.3	491.2, 540.9	514.0	508.3, 552.3
	10% amino acid solution	520.1	517.1, 568.0	507.2	501.4, 546.5
	18% calcium solution	608.9	603.3, 653.0	500.5	497.1, 542.5
	20% lipid emulsion	473.8	467.8, 522.6	502.5	493.1, 542.7

HU, Hounsfield Unit; IQR, interquartile range; IRA, iodine-related attenuation; VME, virtual monoenergetic image

Measurement variability of IoD

As the variables of CT scanners, solvents, and radiation dosage settings were not associated with absolute IoD measurement error, pooled analyses of all data regardless of those variables were performed. In other words, the measurement variability range was calculated for each true iodine concentration. The 2.5 and 97.5 percentiles of absolute IoD measurement error were as follows: -0.6 and 0.4 mg/ml for the true iodine concentration 0 mg/ml; -0.7 and 0.2 mg/ml for the true concentration 1.0 mg/ml; -0.7 and 0.4 mg/ml for the true concentration 2.5 mg/ml; -0.8 and 0.7 mg/ml for the true concentration 5.0 mg/ml; -1.1 and 1.1 mg/ml for the true concentration 10.0 mg/ml; and -1.6 and 1.3 mg/ml for the true concentration 20.0 mg/ml (Table 7).

Table 7. Measurement Variability Range of the Iodine Density on DECT

True iodine concentration	**Median of absolute difference (95% CI)**	**2.5 percentile of absolute difference (95% CI)[a]**	**97.5 percentile of absolute difference (95% CI)[a]**
0	0.0 (-0.1, 0.0)	-0.6 (-0.7, -0.4)	0.4 (0.3, 0.4)
1.0	-0.3 (-0.3, -0.2)	-0.7 (-0.8, -0.6)	0.2 (0.2, 0.3)
2.5	-0.0 (-0.1, 0.0)	-0.7 (-0.8, -0.5)	0.4 (0.3, 0.5)
5.0	-0.4 (-0.2, 0.0)	-0.8 (-0.9, -0.6)	0.7 (0.6, 0.7)
10.0	-0.2 (-0.3, 0.1)	-1.1 (-1.7, -1.0)	1.1 (1.0, 1.1)
20.0	-0.5 (-0.7, 0.2)	-1.6 (-2.0, -1.2)	1.3 (1.2, 1.5)

Iodine density was measured in mg/ml.

[a]95% CIs for the 2.5 and 97.5 percentile values were determined by using bootstrap resampling.

CI, confidence interval

Therefore, a cutoff of IoD for the determination of a truly enhancing lesion on DECT would be 0.4 mg/ml. Similarly, cutoffs for the evaluation of true change in IoD at follow-up DECT scan would be as described in the preceding paragraph.

PART II. ANALYSIS OF THE EFFECT OF VARIOUS ACQUISITION PARAMETERS ON IODINE QUANTIFICATION USING A SINGLE DECT SCANNER (DLCT)

MATERIALS AND METHODS

This study was exempt from Institutional Review Board approval at Seoul National University Hospital as no animal or human data were acquired or used.

Phantom design

To obtain CT scans at various acquisition settings, an experimental study using an anthropomorphic chest phantom (multipurpose chest phantom N1 Lungman) and two custom-made iodine phantoms was performed. The original mediastinal structures (heart and pulmonary vessels) of the anthropomorphic chest phantom were replaced with iodine phantoms. Development of the iodine phantoms is described in detail in Part I.

In Part II, two different solvents were used for the dilution of contrast media: 1) distilled water and 2) 10% amino acid solution (Combiflex lipid 1000 inj.). The amino acid solution was chosen to simulate in vivo measurement (32, 33). In a preliminary study, this solution had a mean attenuation of 48 HU at 120 kVp, which was close to the mean attenuation of thymic cysts or incidental anterior mediastinal masses on

non-enhanced CT scans (32, 33). Consequently, two iodine phantoms with different solvents were prepared and each contained six tubes of iodine concentrations ranging from 0 to 20 mg/ml (Figure 4).

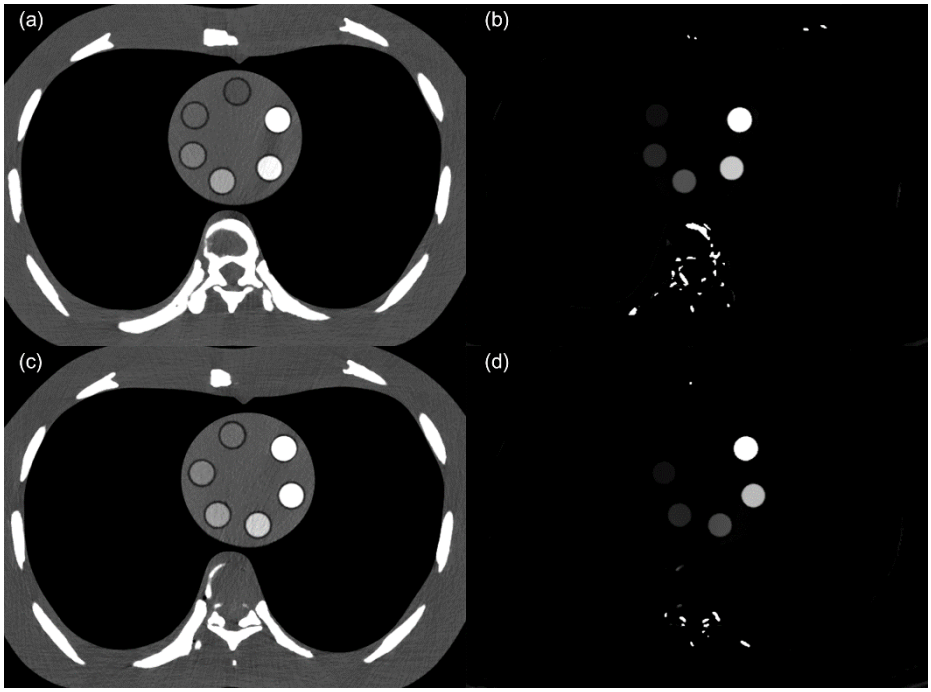

Figure 4. Phantoms designed for iodine quantification. (a) Axial CT image scanned with 140 kVp, 200 mAs and Spectral level 6. A mediastinal iodine phantom containing six tubes approximating different iodine concentrations (contrast media diluted in distilled water; 0, 1, 2.5, 5, 10, and 20 mg/ml) was inserted into an anthropomorphic chest phantom. (b) Iodine density (mg/ml) was measured on the material-specific iodine density image. (c) Another iodine phantom with tubes filled with contrast media diluted in a 10% amino acid solution (iodine concentration: 0, 1, 2.5, 5, 10, and 20 mg/ml) and (d) its iodine density image.

CT acquisition

All CT scans were performed with a DLCT scanner (IQon spectral CT) with modulation of three acquisition variables: tube voltage, tube current-time product, and iterative reconstruction level. The chest phantom was scanned with a voltage of 120 and 140 kVp and a tube current-time product of 20, 40, 60, 80, 100, 150, and 200 mAs. Among Spectral levels (noise-reducing iterative reconstruction levels) from 0 to 7, Spectral 0 and 6 were chosen empirically as these represented low and high noise-reducing levels. Other CT scanning and reconstructing parameters were kept constant as follows: detector collimation, 64x0.625 mm; pitch, 0.984; rotation time, 0.5 sec; slice thickness, 1 mm; reconstruction increment, 1 mm; kernel, B (standard); field-of-view, 310 mm; and matrix size, 512x512 pixels. CT scans were repeated three times for a single acquisition setting with slight position changes between scans. Therefore, a total of 168 CT image datasets (2 kVp settings x 7 mAs settings x 2 Spectral levels x 2 iodine phantoms x 3 repeat scans) were acquired.

Iodine density measurement

CT images were analyzed using the Spectral CT Viewer application of Spectral Diagnostic Suite software (Philips Healthcare) on a workstation (xw6200; Hewlett-Packard) with two 20.8 inch monochrome liquid

crystal display monitors with 2048x1536 pixels (ME315L; Totoku Electric, Tokyo, Japan). IoD was measured by placing round ROIs of approximately 100 mm^2 on three consecutive axial CT images in the middle of the iodine phantoms. Mean IoD (mg/ml) was recorded. Thus, a total of 3024 measurements (168 CT scans x 6 tubes x 3 measurements) were obtained.

Statistical analysis

To investigate the effect of tube voltage, tube current-time product, and Spectral level on IoD measurement, data were analyzed using a linear mixed-effects model. The main effects of interest in the model were the effect of tube voltage, tube current-time product, and Spectral level. Iodine concentrations of phantoms and kind of solvents were also considered as fixed effects. Repeated CT scans were considered as a random effect for interscan variability. The initial models were created with main effects terms with entry of pairwise interaction terms between fixed effects terms iteratively. Thereafter, the final model was created using main effects terms and statistically significant interaction terms.

First, a model with IoD as a dependent variable was constructed. Then, relative iodine measurement error (RME) was used as a dependent variable, calculated as: $\left|(\text{Measured IoD} - \text{True iodine concentration})\right| \times 100/(\text{True iodine concentration})$. Among the input

variables, tube voltage, Spectral level, and kind of solvents were categorical, while tube current-time product was continuous. True iodine concentration was regarded as a categorical variable for the IoD model and as a continuous variable for the RME model as an adjusting factor. Statistical analyses were performed using SAS version 9.2 (SAS Institute Inc., Cary, NC, United States). A P-value <0.05 was considered to indicate statistical significance.

RESULTS

Effect of the acquisition parameters on IoD

In the final mixed-effects model, tube voltage (P<0.001), true iodine concentration of phantoms (P<0.001), and kind of solvents (P=0.007) were statistically significant fixed effects terms. Spectral level (P=0.647) did not have a significant effect on IoD. Tube current-time product was not a significant term by itself (P=0.311). However, two interaction terms associated with the tube current-time product showed statistical significance: interactions between true iodine concentration and tube current-time product (P<0.001), and between tube voltage and tube current-time product (P<0.001). Interactions between true iodine concentration and tube voltage (P<0.001) and between true iodine concentration and kind of solvents were also significant (P<0.001).

To be specific, IoD was measured significantly higher with 140 kVp (Table 8). Absolute differences of least squares means (LSMs) of measured IoD between 120 and 140 kVp, which ranged from 0 to 0.8 mg/ml, increased as true iodine concentration increased. IoD at 140 kVp was closer to the true iodine concentration than that at 120 kVp, except for the 0 mg/ml tube. IoD was also measured significantly higher (and closer to the true iodine concentration) in water than in the amino acid solution for tubes with iodine concentrations ≥5 mg/ml (Table 9). For

tubes with iodine concentration ≤1 mg/ml, IoD was measured lower and less accurately (for 1 mg/ml) in water. LSMs were equal for both solvents at an iodine concentration of 2.5 mg/ml. The difference of LSMs of IoD between water and amino acid solution ranged from 0.1 to 0.3 for tubes with iodine concentrations ≥5 mg/ml and from -0.4 to -0.1 mg/ml for tubes with iodine concentrations ≤1 mg/ml. With regard to the tube current-time product, the estimated regression coefficients were smaller than 0.0005. There was a significantly increasing or decreasing tendency of IoD depending on the interaction between the tube voltage and the tube current-time product. Specifically, the measured IoD decreased significantly as mAs increased at 140 kVp for the tubes with true iodine concentrations ≤2.5 mg/ml. IoD measured at 120 kVp increased significantly as mAs increased for tubes ≥5 mg/ml. Nevertheless, the results implied that the variation in tube current-time product for 100 mAs would cause changes in IoD measurements of smaller than 0.1 mg/ml (Table 10).

Table 8. Iodine Density Measurement according to Tube Voltage

Iodine concentration of phantoms (mg/ml)	**kVp**	**LSM**	**95% CI of LSM**	**Difference of LSM between kVp**	**95% CI of difference**
0	120	0	0, 0		
	140	0.1	0.1, 0.1	0	-0.1, 0
1	120	0.9	0.9, 0.9		
	140	1.0	1.0, 1.0	-0.1	-0.1, -0.1
2.5	120	2.4	2.4, 2.4		
	140	2.5	2.5, 2.5	-0.1	-0.1, -0.1
5	120	4.7	4.7, 4.7		
	140	4.9	4.9, 4.9	-0.2	-0.3, -0.2
10	120	9.4	9.4, 9.4		
	140	9.9	9.8, 9.9	-0.5	-0.5, -0.4
20	120	18.6	18.6, 18.6		
	140	19.4	19.4, 19.4	-0.8	-0.8, -0.8

CI, confidence interval; kVp, kilovoltage peak; LSM, least squares mean

Table 9. Iodine Density Measurement according to the Solvent for Contrast Media Dilution

Iodine concentration of phantom (mg/ml)	Solvent	LSM	95% CI of LSM	Difference of LSM between solvents	95% CI of difference
0	Water	0	0, 0		
	Amino acid	0.1	0.1, 0.1	-0.1	-0.1, -0.1
1	Water	0.8	0.8, 0.8		
	Amino acid	1.1	1.1, 1.2	-0.4	-0.4, -0.3
2.5	Water	2.5	2.5, 2.5		
	Amino acid	2.5	2.5, 2.5	0	0, 0
5	Water	4.9	4.8, 4.9		
	Amino acid	4.7	4.7, 4.8	0.1	0.1, 0.1
10	Water	9.7	9.7, 9.7		
	Amino acid	9.6	9.6, 9.6	0.1	0.1, 0.1
20	Water	19.2	19.2, 19.2		
	Amino acid	18.9	18.9, 18.9	0.3	0.3, 0.3

CI, confidence interval; LSM, least squares mean

Table 10. Coefficients of Tube Current-time Product according to Iodine Concentration and Tube Voltage (Iodine Density Model)

Iodine concentration of phantom (mg/ml)	**kVp**	**Coefficient**	**Standard error**	**P-value**
0	120	0.00010	0.00008	0.224
	140	-0.00021	0.00008	0.008
1	120	-0.00003	0.00008	0.658
	140	-0.00034	0.00008	<0.001
2.5	120	0.00009	0.00008	0.268
	140	-0.00022	0.00008	0.006
5	120	0.00019	0.00008	0.013
	140	-0.00011	0.00008	0.167
10	120	0.00029	0.00008	<0.001
	140	-0.00001	0.00008	0.881
20	120	0.00046	0.00008	<0.001
	140	0.00015	0.00008	0.052

kVp, kilovoltage peak

Effect of the acquisition parameters on RME

Among the fixed effects terms, tube voltage ($P<0.001$), tube current-time product ($P=0.023$), and true iodine concentration ($P<0.001$) were shown to be statistically significant (Figure 5). Kind of solvents ($P=0.053$) and Spectral level ($P=0.813$) were not significant variables. Among pairwise interaction terms, only the interaction between tube voltage and kind of solvents was statistically significant ($P<0.001$).

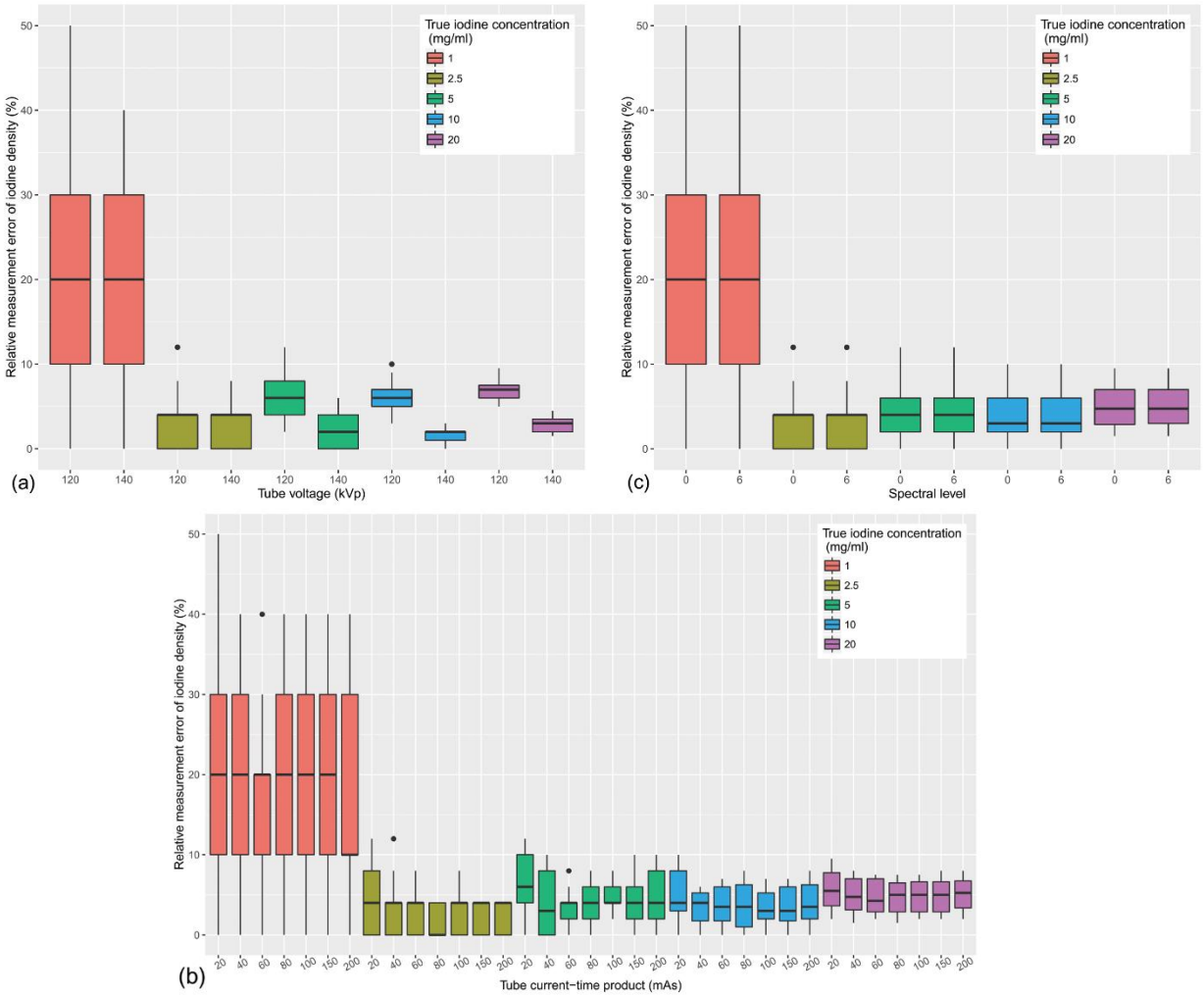

Figure 5. Box plots of relative iodine density measurement error (RME) according to acquisition parameters.

The effect of (a) tube voltage and (b) tube current-time product on RME was minimal. (c) Spectral level was not an influencing factor for RME.

RME decreased significantly as true iodine concentration increased and it was significantly smaller with 140 kVp than with 120 kVp for both solvents (Table 11). The difference of LSMs of RME between 120 and 140 kVp was lower in the amino acid solution (1.0%) than in water (4.2%). RME also reduced as the tube current-time product increased. Given that the regression coefficient was -0.00601 (standard error, 0.00263), an increase or decrease of the tube current-time product for 100 mAs would cause changes in RME of ±0.6%.

Table 11. Relative Iodine Density Measurement Error according to the Solvent and Tube Voltage

Solvent	**kVp**	**LSM**	**95% CI of LSM**	**Difference of LSM between kVp**	**95% CI of difference**
Water	120	9.3	8.7, 9.9		
	140	5.1	4.5, 5.7	4.2	3.3, 5.1
Amino acid	120	7.1	6.5, 7.7		
	140	6.1	5.5, 6.7	1.0	0.1, 1.9

CI, confidence interval; kVp, kilovoltage peak; LSM, least squares mean

PART III. CLINICAL VALIDATION OF IODINE DENSITY MEASUREMENT IN PATIENTS

MATERIALS AND METHODS

This retrospective analysis was approved by the Institutional Review Board of Seoul National University Hospital, and the requirement of written informed consent was waived.

Study population

Patients who underwent chest CT scans using a dedicated scanning protocol for the evaluation of anterior mediastinal lesions between July 2017 and September 2018 were retrospectively identified through searching electronic medical records (EMRs). Among 114 patients, 25 patients underwent surgical resection for the mediastinal diseases. Then, three patients with diseases other than thymic cysts or thymic epithelial tumors were excluded [ectopic thyroid tissue (n=1), mature cystic teratoma (n=1), and schwannoma (n=1)]. Subsequently, 22 patients (12 males and 10 females) with surgically resected thymic cysts (n=14) or thymic epithelial tumors [type A (n=3), AB (n=1), B1 (n=2), and B3 (n=1); subtype was not recorded in one patient] were included for analysis. Median age was 57 years [interquartile range (IQR), 51-67

years]. Median interval between CT scan and surgery was 29 days (IQR, 12-35 days).

CT acquisition

All patients underwent chest CT scans using a single CT scanner (IQon spectral CT; DLCT). Detailed scanning parameters were as follows: 120 kVp; dose right index, 18; detector collimation, 0.625x64 mm; slice thickness, 3 mm; reconstruction increment, 3 mm; rotation time, 0.33 sec; pitch, 1.0015; kernel, B (standard); field-of-view, 150 mm (covering only mediastinum); and matrix size, 512x512 pixels. Patients initially underwent non-enhanced CT scans (limited scan range for the mediastinum to reduce radiation dosage). Then, a total of 1.2 mL/kg of 370 mgI/mL of a nonionic contrast material, iopamidol (Pamiray 370), was injected into an antecubital vein. Contrast-enhanced CT scan was obtained at a scan delay of 60 sec. Both non-enhanced and contrast-enhanced CT scans were also reconstructed at a slice thickness of 1 mm with field-of-view of approximately 350 mm covering the whole thorax, but these were used only for the clinical practice. That is, these CT scans (thin-section and full field-of-view) were not evaluated in this study.

Data collection

Patient characteristics (sex and age), surgery date, and pathological information were recorded from EMRs. All pathological diagnoses were

determined by the attending pathologists of Seoul National University Hospital as a part of routine clinical practice according to the World Health Organization classification (34). Thus, surgical specimens were not reviewed particularly for this study.

Image analysis

CT images were analyzed using the Spectral CT Viewer application of Spectral Diagnostic Suite software (Philips Healthcare). IoD (mg/ml), CT attenuation number (HU) at VME 70 keV (both non-enhanced and contrast-enhanced CT), and CT attenuation number (HU) at VNE were obtained by placing round ROIs on axial images (Figure 6). Mean values were recorded and all measurements were performed once for each patient.

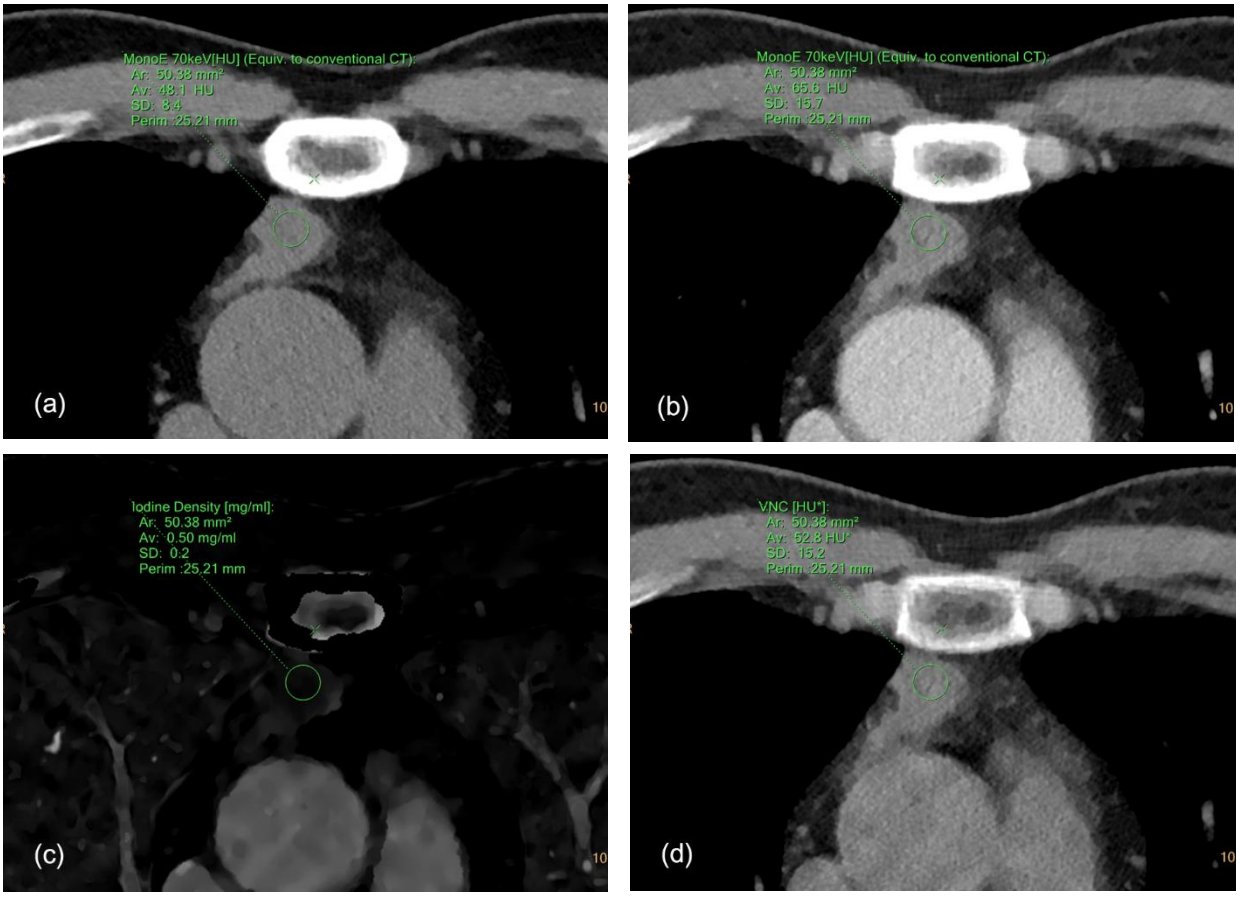

Figure 6. A representative case of a 51-year old male with a thymic epithelial tumor (B3). (a) Non-enhanced VME 70 keV, (b) Contrast-enhanced VME 70 keV, (c) iodine density (IoD) map, and (d) virtual non-enhanced image. Note that IoD was measured as 0.50 mg/ml, which was above the true enhancement cutoff (0.4 mg/ml).

VME, virtual monoenergetic image

Statistical analysis

Continuous variables were described as either mean ± standard deviation or median with IQR after testing the normality with Shapiro-Wilk test. Comparisons of the continuous variables between thymic cysts and thymic epithelial tumors were performed using either independent t-test or Mann-Whitney U test, as appropriate. To validate diagnostic performance of the true enhancement cutoff (IoD, 0.4 mg/ml) in patients, lesions with IoD >0.4 mg/ml were regarded as thymic epithelial tumors, while those with IoD ≤0.4 mg/ml were considered as thymic cysts. In addition, two other diagnostic criteria were adopted for the comparison, which were attenuation cutoffs at VME 70 keV (contrast-enhanced CT) and IRA (HU at contrast-enhanced VME 70 keV minus HU at VNE). Specifically, CT attenuation >20 HU (i.e., water attenuation) at VME 70 keV (35) and IRA >20 HU (36) were used as diagnostic criteria for thymic epithelial tumors, respectively. Diagnostic sensitivity, specificity, accuracy, positive predictive value (PPV), and negative predictive value (NPV) for the differentiation of thymic epithelial tumors from thymic cysts were calculated for each diagnostic criterion. Corrected predictive values for the prevalence of 23.1% (malignant anterior mediastinal disease) at screening chest CT scans, which was recently reported by Yoon et al. (37), were also calculated (38). In addition, diagnostic

sensitivity, specificity, and accuracy were also calculated based on the CT reports, which reflected daily clinical practice of radiologists. When multiple differential diagnoses were suggested at the report, the top differential diagnosis was chosen. The diagnostic accuracies of the attenuation-based cutoffs and the CT report were compared to that of the IoD using McNemar test. All statistical analyses were performed using SPSS Statistics version 25.0 (IBM Corp., Armonk, NY, USA). P-values <0.05 were considered to indicate a statistically significant difference.

RESULTS

Median lesion diameter was 2.2 cm (IQR, 1.7-3.4 cm). Median IoD was 0.22 mg/ml (IQR, 0.12-0.34 mg/ml) in thymic cysts and 1.75 mg/ml (IQR, 0.82-2.67 mg/ml) in thymic epithelial tumors (P<0.001). Median attenuation at non-enhanced VME 70 keV was 20.8 HU (IQR, 12.5-41.1 HU) in thymic cysts and 47.3 HU (IQR, 41.6-52.5 HU) in thymic epithelial tumors (P=0.003). Mean attenuation (±standard deviation) at contrast-enhanced VME 70 keV was 29.2±16.5 HU in thymic cysts and 92.2±26.8 HU in thymic epithelial tumors (P<0.001). Median IRA was 5.6 HU (IQR, 3.3-9.2 HU) in thymic cysts and 44.5 HU (IQR, 20.9-67.8 HU) in thymic epithelial tumors (P<0.001).

Diagnostic performance of the suggested IoD cutoff and attenuation-based cutoffs

Diagnostic sensitivity, specificity, accuracy, PPV, and NPV were 100%, 85.7%, 90.9%, 80.0%, and 100% for IoD (cutoff, 0.4 mg/ml), 100%, 35.7%, 59.1%, 47.1%, and 100% for CT attenuation at contrast-enhanced VME 70 keV (cutoff, 20 HU), and 75.0%, 85.7%, 81.8%, 75.0%, and 85.7% for IRA (cutoff, 20 HU). Disease prevalence (thymic epithelial tumor) was 36.4% (8/22). Corrected PPV and NPV were 67.7% and 100% for IoD, 31.8% and 100% for CT attenuation at contrast-enhanced VME 70 keV, and 61.2% and 91.9% for IRA. Diagnostic

accuracy of IoD was significantly higher than that of the CT attenuation at contrast-enhanced VME 70 keV (P=0.016). However, there was no significant difference between IoD and IRA (P=0.500).

Diagnostic sensitivity, specificity, and accuracy determined based on the radiologist report were 100%, 71.4%, and 81.8%, respectively. The difference in diagnostic accuracy between IoD and the radiologist report was not statistically significant (P=0.625).

Two cases of the thymic cysts were incorrectly diagnosed as thymic epithelial tumors by IoD measurement. In one case, attenuation number at non-enhanced CT was 49.4 HU, although it was erroneously measured as 34.5 HU at VNE, leading to increased IoD (1.04 mg/ml). In another case, a small lesion (1.0 cm) was closely abutting the wall of pulsating ascending aorta and IoD was measured as 1.00 mg/ml. None of the thymic epithelial tumors were misdiagnosed as thymic cysts by IoD measurement. Table 12 is a contingency table for each diagnostic criterion.

Table 12. Differentiation of thymic epithelial tumors from thymic cysts using several diagnostic criteria

		Histopathologic diagnosis (reference standard)	
Diagnostic criteria	**Cutoff**	Thymic cyst	TET
IoD (mg/ml)	≤0.4	12	0
	>0.4	2	8
CT attenuation at contrast-enhanced VME 70 keV (HU)	≤20	5	0
	>20	9	8
IRA (HU)	≤20	12	2
	>20	2	6
Diagnostic CT report of radiologists	Thymic cyst	10	0
	TET	4	8

Data are number of patients.

HU, Hounsfield units; IoD, iodine density; IRA, iodine-related attenuation; TET, thymic epithelial tumor; VME, virtual monoenergetic

DISCUSSION

In Part I, this study revealed that IoD measurement accuracy for the simulated mediastinal cystic lesions was not significantly affected by DECT systems, although the absolute measurement error was slightly higher for SSCT. Fluid characteristics (solvents) did not have any significant impact on IoD, either. For the variability range of IoD, the cutoff for determining a truly enhancing lesion was 0.4 mg/ml, which implied that the measured IoD >0.4 mg/ml could be reproducibly regarded as true contrast-enhancement on DECT scans. In Part II, this study found that tube voltage and tube current-time product had minimal effects on IoD and RME, although both reached statistical significance. The estimated differences between kVp settings ranged between 0 to 0.8 mg/ml for IoD and between 1.0% to 4.2% for RME. As for the tube current-time product, alteration of 100 mAs caused changes in IoD and RME of approximately 0.1 mg/ml and 0.6%, respectively. In addition, among the analyzed variables, Spectral level was not an affecting factor for iodine quantification. In Part III, diagnostic performance of the true enhancement cutoff (IoD, 0.4 mg/ml) was validated in patients who underwent thymectomy and the suggested threshold showed diagnostic sensitivity, specificity, and accuracy of 100%, 85.7%, and 90.9%, respectively.

Recently, Pelgrim et al. (25) performed comparisons between DLCT and DSCT for the iodine quantification and reported that the lowest measurement errors were observed for DSCT with the tube voltage settings of 70/Sn150 kVp or 80/Sn150 kVp, of which the median relative measurement errors for true iodine concentrations ranging from 5.0 to 20.0 mg/ml were 0.5% (range of median: -4, 1%) and -2.3% (range of median: -4, 0%), respectively. The median measurement error for DLCT, acquired with 140 kVp, was -3.3% (range of median: -6, -2%). In the present study, the median relative measurement errors ranged from 5.0% to 8.0% for DSCT and from -7.0% to -4.5% for DLCT for the equal range of iodine concentrations. The measurement errors for DSCT were more overestimated and were higher than those reported by Pelgrim et al. (25). Such discrepancy might be explained by the following reasons. First, the uncertainty of true iodine concentration of the phantoms would be a cause. Commercial contrast media was diluted in order to prepare the iodine phantoms. The ground truth concentration of the contrast media was not tested in both studies. Variation of the concentration of the contrast media might have contributed to the inconsistency of the results. To solve this issue, precise measurements of the true iodine concentration using high-performance liquid chromatography is required. Second, this study dealt with iodine solutions diluted in various solvents

including amino acid solution, lipid emulsion, and calcium solution. DSCT performs three-material decomposition in image space with pre-specified material specific attenuation profiles. Thus, the analysis of complex solutions would inevitably yield a higher measurement error. Third, the CT system calibrations might have affected the IoD measurement. Material decomposition requires accurate system calibrations, which establish the relationship between the projection measurements and known densities of basis materials (2). A slight difference in CT calibration status might have resulted in the disparate results between the two studies. DSCT system was calibrated by the manufacturer three days before the CT scanning in this study.

An interesting finding in Part I was that the absolute measurement error of IoD was not significantly affected by the solvent in which the contrast media was diluted. Given that in vivo lesions such as bronchogenic cyst or thymic cyst comprise complex proteinaceous fluid, it would be possible to suggest that IoD measurement is applicable to the differential diagnosis of in vivo lesions. To my knowledge, this is the first study to investigate the feasibility of IoD measurement using simulated body fluids. Past research on the accuracy of IoD using DECT scanners performed analysis with iodinated contrast media diluted in only water (10, 23, 25, 39) and thus was not able to demonstrate whether the IoD

could be accurately measured for body fluids or body materials.

Considering the study results in Part I, iodine quantification is more robust than attenuation measurement across various DECT platforms and fluid characteristics. Present study results are promising given that the CT scans were obtained from the three major vendors.

With regard to the measurement variability of IoD, a non-parametric form of 95% limits of agreement was calculated for the absolute measurement error (31). This method is very simple but effective and readily interpretable (31). Based on the study results, IoD greater than 0.4 mg/ml can be interpreted as true contrast-enhancement. This would be helpful for the differential diagnosis of a thymic cyst or a renal cyst as demonstrated in Part III. Determination of an enhancing component (i.e., viable tumor) is key to the diagnosis of these lesions and IoD measurement may facilitate radiologic diagnosis when using the suggested cutoff value.

In Part II, DLCT was used for the image acquisition. DLCT enables spectral separation of photons at a detector level (40). Therefore, this scanner does not require setting up of a specific DECT mode for acquisition with different photon spectra. Rather, all routine CT scans achieved for clinical purposes are able to be reviewed retrospectively as DECT when using dedicated software. Nevertheless, little has been

known to date on whether iodine quantification can be affected by changes in CT acquisition parameters with this scanner. Thus, to guarantee that measured values are robust irrespective of the scanning protocols (or acquisition parameters) used, investigation of the effects of acquisition settings on quantification was warranted. Study Part II covered an extensive variation of acquisition settings, especially mAs, to simulate various CT protocols for the purposes of answering this question.

An important finding of the Part II was that selection of 140 kVp yielded higher as well as more accurate IoD measurement; the higher tube voltage may have resulted in more photons detected at the outermost detector layer, which absorbed high-energy photons (25). Thus, a wider spectral separation, leading to more accurate material decomposition, became possible. Nonetheless, the estimated differences in IoD between the two kVp settings were 0.1 mg/ml for the 1 mg/ml tube, 0.1 mg/ml for the 2.5 mg/ml tube, and 0.8 mg/ml for the 20 mg/ml tube. Based on the in vivo measurements reported in the literature, the differences of IoD between the control and disease groups were approximately 0.93 mg/ml for thymoma (median IoD: low-risk thymoma, 1.92 mg/ml; high-risk thymoma, 0.99 mg/ml) (8), 1.21 mg/ml for myocardium (mean IoD: normal myocardium, 2.56±0.66 mg/ml; infarcted myocardium,

1.35±0.57 mg/ml) (9), and 3.89 mg/ml for a solitary pulmonary nodule (mean IoD: benign nodule, 15.30±6.25 mg/ml; malignant nodule, 19.19±6.44 mg/ml) (15). When compared to the differences in IoD between the control and disease groups in vivo, the alteration of IoD due to kVp would have little clinical impact on the differential diagnosis.

Similarly, the effect of tube current-time product on the measurement of IoD was minimal and was not considered to be clinically relevant according to the present results. To be specific, increasing the tube current-time product from 20 to 200 mAs would result in a change in IoD measurement of 0.1 mg/ml and RME of 1.1%. Thus, despite the statistically significant regression coefficients of mAs, such minimal influence would not bear clinical importance in the radiation dose range of diagnostic CT scans.

With regard to the iterative reconstruction algorithm, noise reduction levels had no impact on IoD measurements. Among Spectral levels 0 to 7, two Spectral levels, 0 and 6, were empirically chosen as ‘low’ and ‘high’ levels of noise reduction, respectively. Nowadays, iterative reconstruction is often incorporated in routine imaging as a dose reduction strategy. Therefore, it is essential to investigate the potential influence of iterative reconstruction on quantitative measurements. In addition, one phantom study previously reported that noise was a critical

factor for accurate iodine quantification on material-specific DECT datasets (41). The present study result that the noise reduction level was not associated with IoD measurement is quite informative, given that the heterogeneity in images caused by the various reconstruction algorithms can be potentially put out of court. Pelgrim et al. (25) also reported a similar result in which the grade of iterative reconstruction was not an influencing factor for IoD measurement in both third-generation dual-source DECT and DLCT scanners. Some controversy remains, however, as Marin et al. (39) stated that a higher grade of iterative reconstruction provided significantly greater accuracy in iodine quantification in a second-generation dual-source DECT scanner. Different iterative reconstruction algorithms used might have caused the discrepancy between the study results as the degree of noise reduction and the underlying mechanisms of action vary substantially among the commercial iterative reconstruction algorithms.

In Part III, the true enhancement cutoff for IoD was validated for the differentiation of thymic epithelial tumors from thymic cysts and the proposed criteria showed good diagnostic performance. McErlean et al. (42) previously reported that intralesional fat, midline location, and triangular thymic shape were more frequently associated with benign thymic lesions including thymic cyst, thymic hyperplasia, benign thymus,

thymolipoma, and benign nodular thyroid hyperplasia, compared with thymic malignancy. However, iodine quantification was not performed in that study. Chang et al. (8) measured iodine concentrations in thymic epithelial tumors and reported that iodine concentration measurement could be used in differentiating between low- and high-risk thymomas and thymic carcinomas. Nevertheless, benign thymic lesions were not included and diagnostic cutoff was not validated in an independent cohort.

Notably, CT attenuation of the thymic cysts was higher than that of water (20 HU) in 50% (7/14). Araki et al. (33) also reported that the mean CT attenuation of thymic cysts was 38 HU on contrast-enhanced CT. Therefore, differential diagnosis of a thymic lesion based on a single phase CT scan is challenging and evaluation solely based on the cutoff for water attenuation would result in substantial false positive diagnoses. In this context, DECT can be a solution as this modality provides VNE images from a single acquisition and enables iodine quantification, a less variable measure as demonstrated in Part I. Nevertheless, corrected PPV for IoD measurement was below 70%, which might result in overdiagnosis and subsequent overtreatment. Therefore, care should be taken in medical decision making and treatment planning based on the iodine quantification. Borderline lesions may require additional imaging

tests such as positron emission tomography or magnetic resonance imaging.

There were several limitations in this study. First, IoD was not measured in patients in Part I and Part II. In vivo measurements were simulated with four different solutions. However, the body material in vivo is more complicated than that produced simply in the laboratory. Solid tumors may comprise dense cellular component, water, blood, calcification, and even gross fatty tissue. Thus, the actual measurement error in vivo would be higher than that analyzed in this study. Second, there are multiple other potential sources of variation for IoD measurement including patient body habitus and respiratory/cardiac motion. Past studies reported that the iodine quantification was significantly influenced by the patient size. (25, 39) Therefore, it is possible that the measurement variability range is wider in large phantoms or patients. Accordingly, the accuracy of IoD measurement reported in the present study may alter for the abdominal applications of DECT. Furthermore, iodine measurements using DSCT and SSCT can be affected by the patient motion as there is a minute gap between the acquisition of low and high energy data. Although motion was not considered in the present study, this is an interesting topic to be investigated in the future. Third, lesion size was not analyzed as a variable in the phantom studies. Lesions that have

smaller axial diameter than the tubes may be vulnerable to the acquisition conditions. Fourth, the most recently developed SSCT, Revolution CT (GE Healthcare), which was not commercially available at the time of this study, was not included in the experiment. Therefore, the performance of the most recent SSCT for iodine quantification was not analyzed. Fifth, image quality assessment was not performed. Image quality of DECT including VME and VNE has been investigated in a number of previous studies (43-47). Comparison of the image quality in terms of spatial resolution and noise spectrum between the three vendors is warranted in the future studies. Sixth, intra- and inter-reader IoD measurement variability was not analyzed. Reproducibility is an important aspect of any measurement analysis. However, this study focused on modeling with acquisition factors to reveal their effects on IoD measurements. According to a previous study, Chandarana et al. (23) had demonstrated that the inter-reader agreement of IoD was excellent (Pearson coefficient, 0.994) with dual-source DECT. Seventh, the clinical validation was performed in a small number of patients and the inclusion of surgically resected cases might have induced selection bias. Thus, a prospective validation in a larger cohort is warranted in the future. Lastly, the value of DECT was not compared with positron emission tomography or magnetic resonance imaging. However, this issue is

beyond the scope of the present study and each imaging modality has distinct merits and demerits.

In conclusion, this study revealed that IoD measurement accuracy was unaffected by the DECT scanners, in contrast to CT attenuation number measurement. IoD measurement was feasible for the various simulated body fluids and the effect of acquisition parameters was minimal in the range of diagnostic CT scans. The variability cutoff for determining a true enhancement was 0.4 mg/ml and this criteria exhibited diagnostic accuracy of 90.9% in differentiating thymic epithelial tumors from benign thymic cysts.

REFERENCES

1. Martin SS, Weidinger S, Czwikla R, Kaltenbach B, Albrecht MH, Lenga L, et al. Iodine and fat quantification for differentiation of adrenal gland adenomas from metastases using third-generation dual-source dual-energy computed tomography. Invest Radiol. 2018;53(3):173-8.

2. McCollough CH, Leng S, Yu L, Fletcher JG. Dual- and multi-energy CT: principles, technical approaches, and clinical applications. Radiology. 2015;276(3):637-53.

3. Goo HW, Goo JM. Dual-energy CT: new horizon in medical imaging. Korean J Radiol. 2017;18(4):555-69.

4. Kang MJ, Park CM, Lee CH, Goo JM, Lee HJ. Dual-energy CT: clinical applications in various pulmonary diseases. Radiographics. 2010;30(3):685-98.

5. Lu GM, Wu SY, Yeh BM, Zhang LJ. Dual-energy computed tomography in pulmonary embolism. Br J Radiol. 2010;83(992):707-18.

6. Zhang LJ, Zhao YE, Wu SY, Yeh BM, Zhou CS, Hu XB, et al. Pulmonary embolism detection with dual-energy CT: experimental study of dual-source CT in rabbits. Radiology. 2009;252(1):61-70.

7. Leithner D, Wichmann JL, Vogl TJ, Trommer J, Martin SS, Scholtz JE, et al. Virtual monoenergetic imaging and iodine perfusion

maps improve diagnostic accuracy of dual-energy computed tomography pulmonary angiography with suboptimal contrast attenuation. Invest Radiol. 2017;52(11):659-65.

8. Chang S, Hur J, Im DJ, Suh YJ, Hong YJ, Lee HJ, et al. Volume-based quantification using dual-energy computed tomography in the differentiation of thymic epithelial tumours: an initial experience. Eur Radiol. 2017;27(5):1992-2001.

9. Delgado Sanchez-Gracian C, Oca Pernas R, Trinidad Lopez C, Santos Armentia E, Vaamonde Liste A, Vazquez Caamano M, et al. Quantitative myocardial perfusion with stress dual-energy CT: iodine concentration differences between normal and ischemic or necrotic myocardium. Initial experience. Eur Radiol. 2016;26(9):3199-207.

10. Koonce JD, Vliegenthart R, Schoepf UJ, Schmidt B, Wahlquist AE, Nietert PJ, et al. Accuracy of dual-energy computed tomography for the measurement of iodine concentration using cardiac CT protocols: validation in a phantom model. Eur Radiol. 2014;24(2):512-8.

11. Iwano S, Ito R, Umakoshi H, Ito S, Naganawa S. Evaluation of lung cancer by enhanced dual-energy CT: association between three-dimensional iodine concentration and tumour differentiation. Br J Radiol. 2015;88(1055):20150224.

12. Schmid-Bindert G, Henzler T, Chu TQ, Meyer M, Nance JW, Jr.,

Schoepf UJ, et al. Functional imaging of lung cancer using dual energy CT: how does iodine related attenuation correlate with standardized uptake value of 18FDG-PET-CT? Eur Radiol. 2012;22(1):93-103.

13. Shimamoto H, Iwano S, Umakoshi H, Kawaguchi K, Naganawa S. Evaluation of locoregional invasiveness of small-sized non-small cell lung cancers by enhanced dual-energy computed tomography. Cancer Imaging. 2016;16(1):18.

14. Son JY, Lee HY, Kim JH, Han J, Jeong JY, Lee KS, et al. Quantitative CT analysis of pulmonary ground-glass opacity nodules for distinguishing invasive adenocarcinoma from non-invasive or minimally invasive adenocarcinoma: the added value of using iodine mapping. Eur Radiol. 2016;26(1):43-54.

15. Xiao H, Liu Y, Tan H, Liang P, Wang B, Su L, et al. A pilot study using low-dose Spectral CT and ASIR (Adaptive Statistical Iterative Reconstruction) algorithm to diagnose solitary pulmonary nodules. BMC Med Imaging. 2015;15:54.

16. Yanagawa M, Morii E, Hata A, Fujiwara M, Gyobu T, Ueda K, et al. Dual-energy dynamic CT of lung adenocarcinoma: correlation of iodine uptake with tumor gene expression. Eur J Radiol. 2016;85(8):1407-13.

17. Aoki M, Hirose K, Sato M, Akimoto H, Kawaguchi H,

Hatayama Y, et al. Prognostic impact of average iodine density assessed by dual-energy spectral imaging for predicting lung tumor recurrence after stereotactic body radiotherapy. J Radiat Res. 2016;57(4):381-6.

18. Baxa J, Matouskova T, Krakorova G, Schmidt B, Flohr T, Sedlmair M, et al. Dual-phase dual-energy CT in patients treated with erlotinib for advanced non-small cell lung cancer: possible benefits of iodine quantification in response assessment. Eur Radiol. 2016;26(8):2828-36.

19. Gupta R, Phan CM, Leidecker C, Brady TJ, Hirsch JA, Nogueira RG, et al. Evaluation of dual-energy CT for differentiating intracerebral hemorrhage from iodinated contrast material staining. Radiology. 2010;257(1):205-11.

20. Mileto A, Nelson RC, Samei E, Jaffe TA, Paulson EK, Barina A, et al. Impact of dual-energy multi-detector row CT with virtual monochromatic imaging on renal cyst pseudoenhancement: in vitro and in vivo study. Radiology. 2014;272(3):767-76.

21. Nute JL, Jacobsen MC, Chandler A, Cody DD, Schellingerhout D. Dual-energy computed tomography for the characterization of intracranial hemorrhage and calcification: a systematic approach in a phantom system. Invest Radiol. 2017;52(1):30-41.

22. Mannil M, Ramachandran J, Vittoria de Martini I, Wegener S,

Schmidt B, Flohr T, et al. Modified dual-energy algorithm for calcified plaque removal: evaluation in carotid computed tomography angiography and comparison with digital subtraction angiography. Invest Radiol. 2017;52(11):680-5.

23. Chandarana H, Megibow AJ, Cohen BA, Srinivasan R, Kim D, Leidecker C, et al. Iodine quantification with dual-energy CT: phantom study and preliminary experience with renal masses. AJR Am J Roentgenol. 2011;196(6):W693-700.

24. Li Y, Shi G, Wang S, Wang S, Wu R. Iodine quantification with dual-energy CT: phantom study and preliminary experience with VX2 residual tumour in rabbits after radiofrequency ablation. Br J Radiol. 2013;86(1029):20130143.

25. Pelgrim GJ, van Hamersvelt RW, Willemink MJ, Schmidt BT, Flohr T, Schilham A, et al. Accuracy of iodine quantification using dual energy CT in latest generation dual source and dual layer CT. Eur Radiol. 2017;27(9):3904-12.

26. Mileto A, Marin D, Alfaro-Cordoba M, Ramirez-Giraldo JC, Eusemann CD, Scribano E, et al. Iodine quantification to distinguish clear cell from papillary renal cell carcinoma at dual-energy multidetector CT: a multireader diagnostic performance study. Radiology. 2014;273(3):813-20.

27. Faby S, Kuchenbecker S, Sawall S, Simons D, Schlemmer HP, Lell M, et al. Performance of today's dual energy CT and future multi energy CT in virtual non-contrast imaging and in iodine quantification: a simulation study. Med Phys. 2015;42(7):4349-66.

28. Fintelmann FJ, Bernheim A, Digumarthy SR, Lennes IT, Kalra MK, Gilman MD, et al. The 10 pillars of lung cancer screening: rationale and logistics of a lung cancer screening program. Radiographics. 2015;35(7):1893-908.

29. Rassouli N, Chalian H, Rajiah P, Dhanantwari A, Landeras L. Assessment of 70-keV virtual monoenergetic spectral images in abdominal CT imaging: a comparison study to conventional polychromatic 120-kVp images. Abdom Radiol (NY). 2017;42(10):2579-86.

30. Albrecht MH, Trommer J, Wichmann JL, Scholtz JE, Martin SS, Lehnert T, et al. Comprehensive comparison of virtual monoenergetic and linearly blended reconstruction techniques in third-generation dual-source dual-energy computed tomography angiography of the thorax and abdomen. Invest Radiol. 2016;51(9):582-90.

31. Bland JM, Altman DG. Measuring agreement in method comparison studies. Stat Methods Med Res. 1999;8(2):135-60.

32. Araki T, Nishino M, Gao W, Dupuis J, Washko GR,

Hunninghake GM, et al. Anterior mediastinal masses in the Framingham Heart Study: prevalence and CT image characteristics. Eur J Radiol Open. 2015;2:26-31.

33. Araki T, Sholl LM, Gerbaudo VH, Hatabu H, Nishino M. Intrathymic cyst: clinical and radiological features in surgically resected cases. Clin Radiol. 2014;69(7):732-8.

34. Travis WD, Brambilla E, Burke A, Marx A, Nicholson AG. WHO classification of tumours of the lung, pleura, thymus and heart. Lyon: International Agency for Research on Cancer; 2015.

35. Carter BW, Okumura M, Detterbeck FC, Marom EM. Approaching the patient with an anterior mediastinal mass: a guide for radiologists. J Thorac Oncol. 2014;9(9 Suppl 2):S110-8.

36. Reiter MJ, Winkler WT, Kagy KE, Schwope RB, Lisanti CJ. Dual-energy computed tomography for the evaluation of enhancement of pulmonary nodules </=3 cm in size. J Thorac Imaging. 2017;32(3):189-97.

37. Yoon SH, Choi SH, Kang CH, Goo JM. Incidental anterior mediastinal nodular lesions on chest CT in asymptomatic subjects. J Thorac Oncol. 2018;13(3):359-66.

38. Weinstein S, Obuchowski NA, Lieber ML. Clinical evaluation of diagnostic tests. AJR Am J Roentgenol. 2005;184(1):14-9.

39. Marin D, Pratts-Emanuelli JJ, Mileto A, Husarik DB, Bashir MR, Nelson RC, et al. Interdependencies of acquisition, detection, and reconstruction techniques on the accuracy of iodine quantification in varying patient sizes employing dual-energy CT. Eur Radiol. 2015;25(3):679-86.

40. Patino M, Prochowski A, Agrawal MD, Simeone FJ, Gupta R, Hahn PF, et al. Material separation using dual-energy CT: current and emerging applications. Radiographics. 2016;36(4):1087-105.

41. Primak AN, Ramirez Giraldo JC, Liu X, Yu L, McCollough CH. Improved dual-energy material discrimination for dual-source CT by means of additional spectral filtration. Med Phys. 2009;36(4):1359-69.

42. McErlean A, Huang J, Zabor EC, Moskowitz CS, Ginsberg MS. Distinguishing benign thymic lesions from early-stage thymic malignancies on computed tomography. J Thorac Oncol. 2013;8(7):967-73.

43. Apfaltrer P, Sudarski S, Schneider D, Nance JW, Jr., Haubenreisser H, Fink C, et al. Value of monoenergetic low-kV dual energy CT datasets for improved image quality of CT pulmonary angiography. Eur J Radiol. 2014;83(2):322-8.

44. Neuhaus V, Abdullayev N, Grosse Hokamp N, Pahn G, Kabbasch C, Mpotsaris A, et al. Improvement of image quality in

unenhanced dual-layer CT of the head using virtual monoenergetic images compared with polyenergetic single-energy CT. Invest Radiol. 2017;52(8):470-6.

45. Purysko AS, Primak AN, Baker ME, Obuchowski NA, Remer EM, John B, et al. Comparison of radiation dose and image quality from single-energy and dual-energy CT examinations in the same patients screened for hepatocellular carcinoma. Clin Radiol. 2014;69(12):e538-44.

46. Tawfik AM, Kerl JM, Razek AA, Bauer RW, Nour-Eldin NE, Vogl TJ, et al. Image quality and radiation dose of dual-energy CT of the head and neck compared with a standard 120-kVp acquisition. AJNR Am J Neuroradiol. 2011;32(11):1994-9.

47. Wichmann JL, Gillott MR, De Cecco CN, Mangold S, Varga-Szemes A, Yamada R, et al. Dual-energy computed tomography angiography of the lower extremity runoff: impact of noise-optimized virtual monochromatic imaging on image quality and diagnostic accuracy. Invest Radiol. 2016;51(2):139-46.

국문 초록

서론: 이 연구는 이중에너지 전산화단층촬영술을(CT) 통한 요오드 정량화에 이중에너지 CT 스캐너, 영상 획득 파라미터, 그리고 액체 성상이 미치는 영향을 분석하고, 측정 변이의 범위(measurement variability)를 계산 및 임상적으로 검증하고자 하였다.

방법: Part I과 II에서는 종격동 팬텀을 스캔하고, 요오드 밀도를(iodine density) 측정하여, 이중에너지 CT 스캐너와 영상 획득 파라미터, 액체 성상의 영향을 linear-mixed effect model로 분석하였다. 요오드 밀도의 측정 변이 범위 또한 계산하였다. Part III에서는 요오드 정량화의 변이 범위를 통해 얻은 참조영증강 기준값의(cutoff) 임상적 유용성을 가슴샘종과 가슴샘 낭종으로 수술적 치료를 받은 환자-대조군 연구를 통해 후향적으로 검증하였다.

결과: Part I에서 요오드 밀도의 절대오차는 이중에너지 CT 스캐너 또는 액체 성상에 영향을 받지 않았다($P>0.05$). 요오드 참값이 0 mg/ml인 경우, 변이 범위는 −0.6 mg/ml에서 0.4 mg/ml였으며, 따라서 참조영증강의 기준값은 0.4 mg/ml로 정의하였다. Part II에서 관전압과($P<0.001$) 관전류($P<0.05$; 교호작용 변수에 따라 P 값에 차이가 있음)는 요오드 정량값에 유의한 영향이 있었으나, 그 영향의 크기, 즉, 회귀계수의 절대값은 매우 작았다. 요오드를

희석한 용매의 성상 역시 유의한 영향이 있었으며(P=0.007), 물과 아미노산 용액 간의 최소제곱평균의 차는 ≥5 mg/ml의 농도를 갖는 튜브에 대해서는 0.1에서 0.3 mg/ml였으며, ≤1 mg/ml의 농도를 갖는 튜브에서는 −0.4에서 −0.1 mg/ml였다. 변수 중 스펙트럴 레벨은 측정에 영향을 미치지 않았다 (P=0.647). Part III에서 참조영증강 기준값은(0.4 mg/ml) 환자−대조군 연구에서 가슴샘종과 가슴샘 낭종을 구분하는데 있어 민감도 100%, 특이도 85.7%, 정확도 90.9%, 양성 예측률 80.0%, 음성 예측률 100%를 보였다.

결론: 요오드 밀도는 이종에너지 CT 촬영기계에 영향을 받지 않는 측정값이다. 요오드 밀도는 CT 획득 변수에 유의한 영향을 받으나, 진단적 CT의 범위 내에서 그 영향의 정도는 미미하다. 참조영증강 요오드 밀도 기준값은(0.4 mg/ml) 가슴샘종과 가슴샘 낭종을 정확하게 구분할 수 있는 유용한 파라미터이다.

주요어 : 요오드 정량화, 요오드 밀도, 이중에너지 전산화단층촬영술, 이중층 검출기 전산화단층촬영, 측정 변이, 영상 획득 변수, 가슴샘 낭종

학 번 : 2017−35354